In silico design of a T-cell epitope vaccine candidate for parasitic helminth infection

Ayat Zawawi[1, #a], Ruth Forman[1], Hannah Smith[1], Iris Mair[1], Murtala Jibril[1], Munirah Albaqshi[1], Andrew Brass[2], Jeremy P. Derrick[1,*], and Kathryn J. Else[1,*]

[1]Lydia Becker Institute of Immunology and Inflammation, School of Biological Sciences, Faculty of Biology, Medicine, and Health, University of Manchester, Manchester Academic Health Science Centre, Manchester M13 9PT, United Kingdom,

[2]Faculty of Biology, Medicine and Health, Division of Informatics, Imaging and Data Sciences, The University of Manchester, Manchester, UK.

[#a]Current address: Faculty of Applied Medical Sciences, King Abdul Aziz University, Jeddah, Saudi Arabia.

*Corresponding author

Email: Kathryn.j.else@manchester.ac.uk or Jeremy.derrick@manchester.ac.uk

Abstract

Trichuris trichiura **is a parasite that infects 500 million people worldwide, leading to colitis, growth retardation and Trichuris dysentery syndrome. There are no licensed vaccines available to prevent *Trichuris* infection and current treatments are of limited efficacy. *Trichuris* infections are linked to poverty, reducing children's educational performance and the economic productivity of adults. We employed a systematic, multi-stage process to identify a candidate vaccine against trichuriasis based on the incorporation of selected T cell epitopes into virus-like particles. We conducted a systematic review to identify the most appropriate *in silico* prediction tools to predict histocompatibility complex class II (MHC-II) molecule T-cell epitopes. These tools were used to identify candidate MHC-II epitopes from predicted ORFs in the *Trichuris* genome, selected using inclusion and exclusion criteria. Selected epitopes were incorporated into Hepatitis B core antigen virus-like particles (VLPs). A combined VLP vaccine containing four *Trichuris* MHC-II T-cell epitopes stimulated dendritic cells and macrophages to produce pro-inflammatory and anti-inflammatory cytokines. The VLPs were internalized and co-localized in the antigen presenting cell lysosomes. Upon challenge infection, mice vaccinated with the VLPs+T-cell epitopes showed a significantly reduced worm burden, and mounted *Trichuris*-specific IgM and IgG2c antibody responses. The protection of mice by VLPs+T-cell epitopes was characterised by the production of mesenteric lymph node (MLN)-derived Th2 cytokines and goblet cell hyperplasia. Collectively our data establishes that a combination of *in silico* genome-based CD4+ T cell epitope prediction, combined with VLP delivery, offers a promising pipeline for the development of an effective, safe and affordable helminth vaccine.**

Author Summary

The soil transmitted helminth *Trichuris trichiura* is a major parasite in developing countries; development of a comprehensive vaccine has been elusive. Here we used a systematic approach based on *in silico* identification of MHC-II T cell epitopes from genome sequences, their incorporation into a virus-like particle (VLP), characterization of the assemblies and testing in an *in vivo* murine infection model. Animals vaccinated with a preparation of four different VLP-antigen fusions showed significant reductions in intestinal worm burdens and associated antibody responses consistent with protection. The results suggest that a pipeline based on *in silico* prediction of potent MHC-II T cell epitopes, followed by incorporation into VLPs, could be a strategy which enables rapid translation into a vaccine against *Trichuris trichiura*.

98 ## Introduction

99

100 Trichuriasis, caused by the whipworm *Trichuris trichiura*, is one of the most widespread soil-
101 transmitted helminths (STH) in the world (1). Global mass drug administration (MDA)
102 programmes are being implemented, but cure rates are low, repeated treatments are costly
103 and may prevent the development of acquired immunity. Further, the existence of drug-
104 resistant parasites is a constant concern (2-4). Using the mouse model of human trichuriasis,
105 *Trichuris muris* excretory/secretory (ES) products (5), ES fractions (6), extracellular vesicles
106 (EVs) (7), and, more recently, *T. muris* whey acidic protein (8) in the context of the adjuvant
107 alum, have shown considerable potential in a number of pre-clinical protection trials. Despite
108 these successes, developing a vaccine based on native antigens is associated with many
109 manufacturing challenges, including cost, time consumption, difficulties in purifying large
110 quantities of worm antigens and control over differences between batches (9, 10). The advent
111 of the genome era has provided alternative strategies for vaccine development (11). For
112 example, the reverse vaccinology (RV) approach combines genome information with
113 immunological and bioinformatics tools to overcome some of the limitations of conventional
114 methods of screening vaccine candidates (12-14).
115 These observations, combined with the economic challenges of producing a low-cost vaccine,
116 prompted us to examine the potential of using virus-like particles (VLPs) as a scaffold for the
117 presentation of predicted *Trichuris* MHC-II epitopes. The Hepatitis B core protein (HBc) has
118 been widely used as a VLP: it forms stable self-assemblies, which can accommodate T cell
119 epitopes, is cheap to produce and is safe for human use (15, 16). Structural analysis has
120 shown that each HBc monomer forms helical structures, which protrude as spikes from the
121 capsid (17). Antigens, in the form of short T cell epitopes or whole globular domains, can be
122 inserted at the tip of each spike. Designing vaccines based on 'multi-stage' antigens which
123 are expressed at different stages of infection have shown promising results against several
124 complex pathogens, such as *M. tuberculosis* and *Plasmodium* (18, 19). Further, CD4+ Th2

125 cells play essential roles in the development of protective immunity against *Trichuris* spp
126 (20).The principal objective of this study was therefore to develop a novel MHC II T-cell
127 epitope-based vaccine predicted from multi-stage *Trichuris* proteins, which will induce Th2
128 protective immunity. To achieve this aim, first, a systematic review was performed to select
129 the optimal MHC class II *in silico* prediction tools. Second, potential *Trichuris* MHC-II T-cell
130 epitope vaccine candidates obtained from the *Trichuris* genome were identified using the
131 selected *in silico* prediction tool. Third, these epitopes were produced in a commercially viable
132 manner by fusing epitopes in the hepatitis B core antigen (HBc-Ag) virus-like particle (VLP)
133 vaccine delivery system. These VLPs+T-cell epitope vaccine candidates were then tested *in*
134 *vitro* for their ability to activate antigen presenting cells (APCs). Finally, *in vivo* experiments
135 were conducted to test the protective capacity of VLPs expressing different *Trichuris* T-cell
136 epitopes *in vivo* using *T. muris* infection of mice. Collectively the results of this research
137 represent the first significant progress towards identifying a novel, epitope-based vaccine for
138 trichuriasis.
139

140 ## Results

141

142 **The IEDB and NetMHC-II 2.2 tools exhibited similarly high levels of sensitivity**
143 **for predicting epitopes with strong affinities.** Based on a list of search terms
144 (Supplementary Table S1) used on Google and other websites (Supplementary Table S2), 88
145 servers that predict T-cell epitopes based on MHC class I and II binding were identified
146 (Supplementary Table S3). Of these 88, only 48 tools which could predict MHC-II epitopes
147 were identified. Since our primary focus was MHC-II T-cell epitope prediction, only tools with
148 that functionality were further evaluated using the inclusion criteria (Fig 1A). Five tools met the
149 inclusion criteria: IEDB, SYPEITHI, NetMHC-II 2.2, Rankpep and ProPred. These tools were
150 then scanned for the ability to predict MHC-II T-cell epitopes for two mouse alleles, I-Ab and
151 I-Ad. The ProPred tool was excluded from further analysis because it only predicted HLA-DR

152 binding sites. The four epitope prediction tools that met all the selection criteria were
153 subsequently evaluated using an epitope training set to calculate the sensitivity with which
154 they could predict MHC II T-cell epitopes. Using the epitope training set (Supplementary Table
155 S4), it was observed that IEDB and NetMHC-II 2.2 tools had high levels of sensitivity
156 (~78.00%) for predicting MHC-II T-cell binding epitopes with high affinities, while Rankpep and
157 SYFPETHI exhibited low sensitivity (10.61% and 8.33%, respectively). Collectively, the data
158 indicate that the best prediction tools across all MHC-II T-cell prediction servers considered in
159 this study are IEDB and NetMHC-II 2.2.

160 **Data acquisition and identification of potential vaccine component proteins.** The
161 stichosome, which forms the majority of the whipworm anterior region, is thought to release
162 ES products which trigger the host immune response and induce host immunity after infection
163 (7, 21). Research conducted by Dixon et al., (22) and Else et al., (23), showed that antibody
164 recognition of high molecular weight proteins in both *T. muris* adult and larval ES correlated
165 with resistance to *T. muris* infection. To increase the chances of the identification of antigens
166 which induce a strong immune response, secreted and surface-exposed proteins associated
167 with the anterior region of L2, L3, male and female adult worms were selected for this study
168 (24).

169 Predicted ORFs from the 85-Mb genome (~11,004 protein-encoding genes) of *T. muris* and
170 the 73-Mb genome (~9650 protein-coding genes) of *T. trichiura* (24) were scanned for
171 potential vaccine candidates; 637 proteins were selected. From this subset, only proteins that
172 possess signal peptides and did not exhibit transmembrane domains were included, reducing
173 the total to a sample of 156 proteins. Full-length sequences of the *Trichuris* proteins were
174 obtained from the Universal Protein Resource (UniProt) database in FASTA format
175 http://www.uniprot.org/.

176 **Elimination of closely homologous mouse and human proteins.** To eliminate
177 potential autoimmune reactions when tested in mice and humans, the 156-protein subset was
178 checked to determine homology with human and mouse proteins using the basic local

179 alignment search tool (BLAST). All proteins with any degree of homology with humans or mice
180 were excluded, leaving 60 candidate proteins. Of these, only upregulated proteins in the
181 anterior region of L2, L3 and adult worms were selected based on their transcript expression
182 level. This criterion was based on high-throughput transcriptome data generated from the RNA
183 of *T. muris* and Gene Ontology (GO) term enrichment analyses, a transcriptional upregulation
184 in a particular protein refers to a ≥10 Log2 (normalised read count) transcript expression level
185 (24). Implementing this criterion, 27 proteins were selected for MHC-II T-cell epitope prediction
186 (Fig 1B).

187 **Prediction of *Trichuris* MHC-II T-cell binding epitopes.** All 27 selected proteins were
188 screened to predict T-cell MHC class II epitopes using the IEDB (consensus method)
189 prediction tool (25). The analysis was carried out to predict the binding affinity to the MHC
190 class II allele I-Ab mouse strain and the 11 most prevalent human class II HLA allele
191 supertypes (25-28). The consensus method was used to select only those peptides with a low
192 median percentile rank according to three different prediction methods to reduce the chance
193 of failure during prediction. To cover common global alleles, peptides were selected based on
194 their ability to bind to at least three different human alleles.

195 **Conservation and allergens.** To assess how well the predicted MHC-II T-cell peptides
196 were conserved within the *T. trichiura* genome, the IEDB conservancy analysis tool was used.
197 This tool calculates the degree of conservancy (i.e. similarity) of a peptide within a specified
198 protein sequence (29). Only peptides that were >70% conserved with at least one homologous
199 *T. trichiura* protein were selected for further analysis. Of the 219 MHC-II T-cell peptides, only
200 33 met these criteria. The 33 MHC-II peptides were then assessed for the prediction of IgE
201 epitopes and allergenic potential using the AllerTOP v.2.0 server http://www.ddg-
202 pharmfac.net/AllerTOP/ (30). The final set of 10 *Trichuris* MHC-II T-cell epitopes containing
203 33 overlapping peptides were predicted to have no allergenic potential. The 10 epitopes were
204 further triaged to a final four epitopes based on solubility once expressed on HBc-Ag VLPs. A

205 flow diagram summarising the approach used is shown in Fig 1B, with the final 4 *Trichuris*
206 MHC II T-cell epitopes detailed in Fig 1C.

207 **Purification and assembly of VLPs expressing *Trichuris* T-cell epitopes.** Four
208 HBc-Ag fusion proteins were designed, incorporating each predicted T-cell epitope into the
209 major immunodominant region. The construct also included a Strep tag at the C-terminus, for
210 affinity purification (Supplementary Figure S1). A second round of purification using size
211 exclusion chromatography was performed to produce a homologous population of assembled
212 VLPs. HBc-Ag preparations expressing *Trichuris* MHC-II T-cell epitopes were pure by SDS
213 PAGE (Supplementry Figure S1 B-E). The endotoxin levels in all purified VLPs used in this
214 study were <0.2 endotoxin units (EU) as assessed using the ELISA-based endotoxin detection
215 assay (Data not shown).

216 **VLPs expressing *Trichuris* T-cell epitopes induced the production of**
217 **proinflammatory cytokines *in vitro* and were internalised and co-localized in**
218 **APCs.** BMDCs stimulated with different VLPs, irrespective of whether they include T-cell
219 epitopes, produced high levels of IL-6 (Fig 2A) and TNF-α (B) at levels equivalent to LPS and
220 ES-stimulated BMDCs. Similiarly, all VLPs activated BMDMs, inducing the secretion of high
221 levels of both TNF-α (Fig. 2E), and IL-6 (F). To visualise VLP internalisation by APCs, BMDCs
222 and BMDMs were stimulated with or without fluorescein-conjugated VLPs. Images of
223 individual cells taken by merging the brightfield (BF) and FITC (green) channels demonstrated
224 that the fluorescein-conjugated VLPs were internalised by both APCs (Fig 2C & G). To confirm
225 that the VLPs were co-localized within the APC lysosome and not the cell surface, BMDCs
226 and BMDMs were stained with the lysosome-specific LysoTracker dye. Cells were then
227 subsequently stimulated with or without fluorescein-conjugated VLPs. Merged images of the
228 brightfield (BF), FITC (green), and Lysotracker (red) channels revealed that the fluorescein-
229 conjugated VLPs were accumulated in the lysosome compartment of the BMDCs (Fig 2D) and
230 BMDMs (Fig 2H).

231 **Immunization of mice with VLPs expressing *Trichuris* T-cell epitopes induced a**
232 **significant reduction in worm burden following challenge infection.** The protective
233 capacity of the 4 T cell epitopes was assessed in the *T. muris* – mouse accelerated expulsion
234 model (31) (Fig 3A). Mice vaccinated with pre-mixed four VLPs+T-cell epitopes showed a
235 statistically significant reduction in worm burden by day 14 p.i. compared to the native VLP
236 (HBc-Ag; ($P<0.01$) and PBS ($P<0.05$) immunised groups (Fig 3B). In comparison, ES/Alum
237 immunised mice harboured no parasites (Fig 3C).
238 **Immunization of VLPs expressing *Trichuris* T-cell epitopes induced humoral**
239 **immunity following challenge infection.** To evaluate *T. muris* - specific serum antibody
240 responses induced by vaccination with VLPs+T-cell epitopes, parasite-specific IgM, IgG1, and
241 IgG2c serum antibody levels were determined at d14 p.i. Following vaccination and infection,
242 VLPs+T-cell epitopes and ES/Alum vaccinated mice had statistically significant higher levels
243 of parasite-specific IgM (Fig 3D) and IgG2c (F) compared to the control PBS and native VLP
244 (HBc-Ag) injected mice. However, high levels of parasite-specific IgG1 were only detected in
245 the serum of mice vaccinated with ES/Alum following *Trichuris* infection (Fig 3E). There was
246 no or very low levels of parasite-specific IgM, IgG1, and IgG2c detected in the serum of native
247 VLP (HBc-Ag) and PBS/alum injected mice at day 14 p.i., as shown in Fig. (3D-F). Similarly,
248 statistically significant higher levels of VLPs+T-cell epitopes-specific IgM (Fig 3G), IgG1 (H)
249 and IgG2c (I) were produced following *Trichuris* infection of mice vaccinated with VLPs+T-cell
250 epitopes, compared to mice given native VLP (HBc-Ag) or PBS. Notably, mice vaccinated with
251 ES/Alum also produced high levels of VLPs+T-cell epitopes-specific IgM following *Trichuris*
252 infection, as shown in Fig 3 (G).
253 **Immunisation of mice with VLPs expressing *Trichuris* T-cell epitopes induces a**
254 **mixed Th1/Th2 immune response following challenge infection.** To analyse the
255 cellular immune responses at the primary site of adaptive immune cell activation following *T.*
256 *muris* infection (32), MLN cells of mice vaccinated with VLPs+T-cell epitopes were re-
257 stimulated *in vitro* with *Trichuris* ES. Supernatants were assayed for Th2 cytokines (IL-4, IL-5,

258 IL-9 and IL-13), Th1/Th17 cytokines (IL-2, IFN-γ and IL-17), proinflammatory cytokines (IL-6
259 and TNF-α), and the anti-inflammatory cytokine (IL-10) production by CBA (Fig 4 and
260 Supplementary Figure S2). Levels reached significance versus control vaccinated mice for IL-
261 5 (Fig 4A; ES vaccinated mice) and IFN-γ (Fig 4D; VLP+T cell epitope vaccinated mice) with
262 non-significant increases in IL-9 and IL-13 (Fig 4B, 4C). MLN cells from all vaccinated mouse
263 groups also produced IL-4, IL-6, IL-10, IL-17 and TNF upon their re-stimulation *in vitro*
264 (Supplementary Figure S2 A-E). Collectively these data support the *in vivo* immunogenicity of
265 the novel VLP+ T cell epitope vaccine, evidencing the presence of a mixed Th1/Th2 immune
266 response and are in keeping with the worm expulsion and antibody data. Proximal colon
267 goblet cells were quantified in mice vaccinated with ES/Alum, PBS, VLP (HBc-Ag) and
268 VLPs+T-cell epitopes day 14 post *T. muris* infection. (Fig 4E). Interestingly, VLPs+T-cell
269 epitopes and ES/Alum vaccinated mice exhibited a significantly elevated goblet cell
270 hyperplasia ($P<0.05$) compared to mice injected with PBS or native VLP (HBc-Ag) (Fig 4F).
271

272 ## Discussion

273

274 *Trichuris trichiura* is one of the most common human STH parasites and remains a major
275 health concern for humans worldwide (1). A number of pre-clinical vaccines against trichuriasis
276 have been reported, containing whole *Trichuris* antigens or fractions (6, 7, 22). However,
277 developing a vaccine for *Trichuris* based on native antigens has several limitations (10). An
278 alternative strategy embraces the use of informatics to predict and assess MHC-II T cell
279 epitopes using criteria to maximize their *in vivo* protective potential. The fast-growing
280 application of VLP-based vaccines against several parasites, including *Plasmodium* spp (33,
281 34), *Leishmania infantum* (35), *Toxoplasma gondii* (36), *Trichinella spiralis* (37), and
282 *Clonorchis sinensis* (38) prompted our interest in developing a VLP-based vaccine against
283 trichuriasis.

284 **Identification of novel *Trichuris* MHC-II T-cell epitopes as promising vaccine**
285 **candidates.** Initiation of an antigen-specific immune response requires presentation of
286 antigenic peptides to CD4+ T-cells in the context of MHC Class II molecules (39). Selection
287 of appropriate MHC Class II binding peptides is therefore a critical first step in developing an
288 epitope-based vaccine. There are more than 80 computer-based prediction tools for
289 identifying peptides that bind to MHC class I and II molecules, but not all are equivalent; some
290 epitope prediction tools may fail to predict all significant epitopes (40). The performance of *in*
291 *silico* prediction tools is affected by several factors. For example, MHC-II CD4+ T-cell epitope
292 prediction tools have much lower accuracy than MHC-I tools because the MHC-I binding
293 groove is closed, while the MHC-II groove is open at both ends (40, 41). Also, the use of a
294 limited training dataset to evaluate the tools may affect performance (25, 42, 43). Further, the
295 low performance of MHC class II prediction tools may not only be due to poor algorithm
296 performance; the genetic diversity of human populations presents additional challenges (44).
297 Thus, choosing the best bioinformatics tool to predict MHC class II T-cell epitopes is critical
298 when designing epitope-based vaccines (45, 46). This study presents a systematic review of
299 existing MHC-II restricted T-cell epitope prediction tools and evaluated four tools in order to
300 establish the most appropriate bioinformatics tools currently available for predicting *Trichuris*
301 MHC-II T-cell epitopes.
302 The IEDB and NetMHC-II 2.2 tools achieved similarly high levels of sensitivity of predicting
303 binding epitopes with high affinities, while Rankpep and SYFPETHI exhibited low sensitivity.
304 Each tool applies different methods of prediction; the IEDB tool uses a quantitative consensus
305 method that combines the strengths of various methods (25); the NetMHC-II 2.2, another
306 quantitative tool, uses an NN-align algorithm and weight matrix (28); and both SYFPEITHI (47)
307 and Rankpep (48) are qualitative tools that use motif PSSMs. All the tools were 'user-friendly'
308 but SYFPETHI was limited in its coverage of mouse and human MHC-II alleles. The IEDB tool
309 has features that the other three do not, including a browser to input protein sequence formats

310 in a National Centre for Biotechnology Information (NCBI) database, seven different prediction
311 methods and an easy method of downloading the prediction output into an Excel spreadsheet.
312 Several studies have compared the performance of different MHC class II peptide binding
313 prediction tools (49-51), but the comparison presented in this study is different for two main
314 reasons. First, the MHC-II prediction tools were selected in a systematic way using
315 inclusion/exclusion criteria. Second, a unique dataset consisting of a new 'test' dataset which
316 has not been used to build or evaluate IEDB was used. For example, Zhao and Sher (2018)
317 evaluated the MHC-II prediction tools hosted on the IEDB analysis resource server using
318 newly available, untested data of both synthetic and naturally processed epitopes. Among the
319 18 predictors that were benchmarked, NetMHC-II outperformed all other tools, including
320 NetMHCIIpan and the consensus method for both MHC class I and class II predictions (52).
321 Furthermore, Andreatta et al. (2018) created an automated platform to benchmark six
322 commonly used MHC class II peptide binding prediction tools using 59 datasets that were
323 newly entered into the IEDB database and had not yet been made public to prevent biased
324 assessment of the available prediction tools. Their evaluation suggested that NetMHCIIpan is
325 currently the most accurate tool, followed by NN-align and the IEDB (consensus) tool (53).
326 Despite differences in the datasets used for comparison, these studies agree with the
327 comparison study conducted in our study, which found that the IEDB (consensus) and
328 NETMHC-II 2.2 (ANN) tools are among the best MHC-II prediction tools. However,
329 NetMHCIIpan could not be included in this study because it did not meet the inclusion criteria.
330 Collectively, we recommend the use of IEDB and NETMHC-II 2.2 prediction tools in any MHC
331 class II epitope prediction study to reduce the experimental cost of identifying epitopes.
332 However, the output of these tools needs to be carefully evaluated *in vitro* and *in vivo* before
333 they are used to bring an epitope-based vaccine to trial.
334 Since the advent of immunoinformatics tools for prediction of antigenic epitopes and protein
335 analysis, several VLP-based vaccines have been engineered to carry foreign antigens and
336 have proven to be highly immunogenic (54). To our knowledge, the data presented in this
337 study is the first to identify novel *Trichuris* MHC-II T-cell epitopes as potential vaccine antigen

338 candidates. The framework used here to identify potential epitope vaccine candidates within
339 the *T. muris* and *T. trichiura* genome could be used in the future to identify potential vaccine
340 candidates for other parasite species. The final set of *Trichuris* MHC-II T-cell epitope vaccine
341 candidates were derived from chitin-binding domain-containing proteins and chymotrypsin-like
342 serine proteases (Fig 1C).
343 Chitin-binding domains genes are highly expressed in different life stages in many nematodes
344 including the parasites *T. trichiura*, *Ascaris lumbricoides* and *Ancylostoma ceylanicum* and the
345 free-living nematode *Caenorhabditis elegans*, (55-58). In particular, these proteins are thought
346 to be associated with eggshell formation and early development at the single-cell stage (59,
347 60). Furthermore, given that, in addition to *T. muris*, more than 40 other helminth species
348 express high levels of chymotrypsin-like serine proteases, these proteins may also be
349 promising vaccine candidates for other helminths (24, 61). Chymotrypsin-like serine proteases
350 are thought to play central roles in either the invasion process or modulation of the host
351 immune response to enhance parasite survival (62-65). In addition, numerous publications,
352 using pre-clinical models of parasitic infection, have noted that protective immunity can be
353 consistently achieved using helminth protease molecules (66). For example, vaccinating
354 BALB/c mice with the whole recombinant serine protease of *T. spiralis* prior to challenge
355 infection led to a reduction in worm burden and induced a mixed Th1/Th2 immune responses
356 (67-69). Furthermore, Shears et al. (6) showed that vaccinating mice with the *T. muris* ES
357 fraction containing serine proteases induced high parasite-specific antibody responses.
358 Remarkably all the proteins selected in this study have been identified within the most
359 immunogenic fractions of *T. muris* ES following vaccination of mice (6).
360 **Identification of a novel VLP-based vaccine against trichuriasis.** All VLP
361 recombinant proteins stimulated a non-specific inflammatory response characterized by the
362 secretion of high levels of proinflammatory cytokines. Furthermore, by identification of
363 intracellular co-localization with lysosomes, VLPs were shown to be taken up by both BMDC
364 and BMDMs. These results are consistent with those of Serradell et al. (70) and Wahl-Jensen

365 et al. (71) who examined the activation of APCs in response to VLPs. For example, Serradell
366 et al. developed a (VLP-HA/VSP-G) vaccine composed of an influenza virus expressing
367 influenza virus hemagglutinin (HA) antigen, co-expressed with the extracellular region of
368 *Giardia lamblia* variant-specific surface proteins (VSPs) as an adjuvant. The recombinant
369 protein (VLP-HA/VSP-G) induced the secretion of high levels of TNF-α, IL-10, and IL-6
370 cytokines *in vitro*. They also showed that oral vaccination with the recombinant protein
371 protected mice from influenza infection and generated protective humoral and cellular
372 immunity. These results suggest that the VLPs are well placed to act as delivery systems to
373 drive immune responses. Further, the data raises the exciting prospect of modifying the VLPs
374 using adhesion molecules and/or cytokines co-displayed on the VLP surface, in order to target
375 the epitopes to specific APC subsets, thus enhancing the activation of antigen-specific T- cells
376 (72).
377 Remarkably, upon challenge with *T. muris* infection, mice vaccinated with 50 µg of pre-mixed
378 VLP+T-cell epitopes (HBc-CBD$_{1243-1259}$, HBc-CBD$_{241-257}$, HBc-CLSP$_{143-158}$, and HBc-CLSP$_{398-}$
379 $_{416}$), in the absence of any additional adjuvant, showed a significantly reduced worm burden.
380 Parasite-specific IgM and IgG2c were detected in the sera of mice vaccinated with the
381 VLPs+T-cell epitopes. Levels were equivalent to the control ES in alum-vaccinated mice, and
382 significantly higher than control vaccinated and infected mice. These results suggest that
383 these VLPs+T-cell epitopes are antigenic and can boost antibody response sufficiently to
384 recognize specific small peptides in the *T. muris* ES. Importantly, analysis of the serum from
385 immunised mice showed that vaccination with the VLPs+T-cell epitopes elicited high levels of
386 IgM, IgG1 and IgG2c to the VLP+T cell epitope recombinant protein pool (HBc-CBD$_{1243-1259}$,
387 HBc-CBD$_{241-257}$, HBc-CLSP$_{143-158}$, and HBc-CLSP$_{398-416}$) with limited recognition of the native
388 VLP (HBc-Ag) protein. In keeping with these data, the malaria VLP-based vaccine (Malarivax)
389 (73-75) composed of HBc-Ag expressing *P. falciparum* T cell and B-cell epitopes identified
390 from the circumsporozoite protein developed long-lasting immunity, eliciting a CD4+ T cell
391 immune response and is currently undergoing a clinical trial (15, 76, 77). The results of these
392 studies support some critical insights into VLP-based vaccines, including confirming that an

393 HBc virus-like particle, in particular, is an excellent delivery system for developing potential
394 vaccine candidates for parasites.
395 A proportion of mice vaccinated with VLP+T-cell epitopes produced detectable levels of MLN-
396 derived Th2 cytokines IL-5, IL-9, and IL-13 in response to re-stimulation *in vitro* with *Trichuris*
397 ES. The Th1 cytokine IFN–γ was also significantly elevated above levels detected in control
398 mice. These data indicate that vaccine-induced protective immunity is characterized by a
399 mixed Th1/Th2 immune response, as has been previously reported (21, 78). Similarly, Gu et
400 al (78), reported that the protective immunity to *Trichinella spiralis* infection induced by
401 vaccination with CD4+ T cell epitopes was associated with both Th1 and Th2 cytokines.
402 Whilst the mechanism by which vaccination protects mice from *T. muris* infection remains
403 unclear, this study reveals that vaccination of mice with VLPs+T-cell epitopes or ES/Alum
404 promoted a marked goblet cell hyperplasia (79). Goblet cells, and the mucins they produce,
405 have been implicated in Th2-mediated defence in mice resistant to a primary *T. muris* infection
406 (80, 81). However, it remains to be determined whether the goblet cell hyperplasia seen here
407 in vaccinated mice is simply a Th2 correlate or is functionally important in the protection
408 observed. In summary, the current study describes the development and efficacy of a novel
409 epitope-based vaccine against trichuriasis. VLPs expressing different *Trichuris* MHC-II T-cell
410 epitopes, predicted from chitin-binding domain containing proteins and chymotrypsin-like
411 serine proteases, were shown to promote protective immunity *in vivo*. Collectively, given the
412 right combination of immunoinformatics and immunogenicity screening tools, epitope-based
413 vaccines will undoubtedly limit the cost and effort associated with bringing a *Trichuris* vaccine
414 to trial.
415

416 ## Methods

417 **Search strategy.** A protocol was designed to identify the bioinformatics tools that can predict
418 MHC-II T-cell epitopes in accordance with the well-defined Preferred Reporting Items for
419 Systematic Reviews and Meta-Analyses (PRISMA) (82). The search was limited to the English

420 language and used the search terms shown in (Supplementary Table S1). A list of the search
421 terms was first used in December 2015 on Google and other websites (Supplementary Table
422 S2) to screen for MHC class I and II *in silico* prediction tools. The number of citations (>200),
423 number of publications (>200), online availability, last update and community were considered
424 to determine whether the tools would be selected for further analysis. The number of
425 publications and citations for each tool were obtained from Google Scholar. In the case of
426 duplicate citations, the highest number of citations was used. A flow diagram of the systematic
427 review screening process for MHC-II T-cell bioinformatics prediction tools is shown in Fig. 1A.
428 **Construction of an epitope training set.** To evaluate the performance of the tools, a
429 literature search for MHC-II CD4+ T-cell peptide binding datasets was performed using the
430 search terms 'universal T-cell epitopes' and 'MHC class II T-cell epitopes' on Google Scholar
431 in December 2015. These datasets included epitopes with publicly available sequences that
432 the literature had experimentally validated to be immunogenic in mice. Because training sets
433 of peptides were used for the development of epitope prediction tools, care was taken to
434 exclude the training datasets used for tool development (83-85).
435 In order to find the optimal set of epitopes, two different sets of epitopes were analysed. The
436 first set was composed of publicly available series of peptide sequences from 15 different
437 proteins that can bind to MHC class II molecules. The second set included one untested
438 protein of *T. muris*, which served as a control to evaluate the performance of the tools.
439 Collectively, the training dataset was composed of 145 epitopes from 16 different proteins
440 (Supplementary Table S4).
441 **Prediction of *Trichuris* MHC-II T-cell epitopes.** Full-length sequences of proteins containing
442 T-cell epitopes were obtained from the Universal Protein Resource (UniProt) database
443 http://www.uniprot.org in FASTA format. The Immune Epitope Database (IEDB), NetMHC-II
444 2.2, Rankpep and SYFPEITHI tools were used to predict T-cell epitopes for mouse strains
445 with I-Ab and I-Ad mouse alleles. Each tool applied a different prediction method and scoring
446 system to generate the predictions output. For instance, the IEDB tool uses the consensus
447 method for prediction, which combines the NN-align, SMM-align, combinatorial library and

448 Sturniolo methods (25), while the NetMHC 2.2 tool uses ANNs (28). The median percentile
449 rank (%) of the three prediction methods was used to generate the rank for the consensus
450 method. A small numbered percentile rank (%) indicates that a peptide has a high binding
451 affinity to MHC class II alleles (25).The output of the IEDB and NetMHC 2.2 tools (the binding
452 affinities) were expressed as half-maximal inhibitory concentration IC50 (nM) values. Epitopes
453 that bind with an affinity of <50 nM are considered to have high affinity, those that bind with
454 <500 nM have an intermediate affinity and those that bind with <5000 nM have a low affinity
455 (28). All epitopes with high or intermediate affinity are considered 'true binders', while epitopes
456 with low affinity are considered 'nonbinders'. No known T-cell epitope has an IC50 value of
457 >5000 nM (25). The scoring system of the SYFPEITHI prediction tool depends on whether
458 peptide amino acids are frequently occur in anchor positions. Optimal anchor residues are
459 given the value 15 and scores of -1 or -3 points are given to amino acids that have a negative
460 effect on epitopes' binding ability at a certain sequence position. Epitopes that bind strongly
461 are among the top 2% of all peptides predicted in 80% of all predictions results (47). The
462 Rankpep tool uses position-specific scoring matrices (PSSMs) to predict MHC-II T-cell
463 epitopes (48). A high peptide score percentage indicates that the epitope is likely to bind to
464 the set of aligned peptides that bind to a given MHC-II molecule (48). The peptide lengths in
465 all the resulting sets were based on the complex of 15 mer core region peptides of MHC class
466 II molecules.
467 **Evaluation and statistical analysis.** Using the training set of epitopes, the performance of
468 the four MHC-II epitope prediction tools, selected through our inclusion/exclusion criteria, were
469 assessed as weak, intermediate or high binders. The prediction results were classified into
470 two categories, true positive (TP) and false negative (FN), based on the threshold values (86).
471 In addition, the evaluation assessed sensitivity (TP/ [TP+FN]). Nonparametric Spearman
472 correlation and Bland-Altman analyses were performed to show the relationship and
473 agreement between the scores derived from the NetMHC-II 2.2 and IEDB tools. The level of
474 significance was set at $p < 0.05$ for the correlation test.

475 **Mice and Parasites.** 6–8 weeks male C57BL/6 mice (Envigo) were fed autoclaved food and
476 water and were maintained under specific pathogen-free conditions. Parasite maintenance,
477 ES collection from adult *T. muris* worms and the method used for infection and evaluation of
478 worm burden were carried out as described previously (87).
479 **Ethics Statement.** All animal experiments were approved by the University of Manchester
480 Animal Welfare and Ethical Review Board and performed under the regulation of the Home
481 Office Scientific Procedures Act (1986), and the Home Office approved licence 70/8127.
482 **Plasmid construction.** The coding sequence for native VLP (HBc-Ag) was engineered with
483 BamHI + EcoRI sites to allow insertion of peptide antigen sequences into the major
484 immunodominant region (MIR). The entire HBc-Ag coding sequence was inserted into the
485 pET17b expression vector between the NdeI (CATATG) and XhoI (CTCGAG) restriction sites.
486 The insertion of each MHC-II T-cell epitope into the MIR was obtained by annealing the
487 relevant oligonucleotide primers (Supplementary Table S5) with BamHI + EcoRI restriction
488 sites and ligation into BamHI/EcoRI cut HBc-Ag in the pET-17b vector. Constructs containing
489 MHC-II T-cell epitopes were confirmed by DNA sequencing.
490 **Production and purification of VLP recombinant proteins.** The recombinant plasmids
491 were transformed into ClearColi-BL21 (DE3) electrocompetent cells (Lucigen) by heat-shock
492 transformation. The bacterial culture was grown in LB media containing 100 µg/mL ampicillin
493 and incubated at 37°C for 14 hours in a shaker incubator. The transformed cells at a starting
494 optical density (0.1 OD600) were inoculated into LB liquid media supplemented with 100
495 µg/mL ampicillin for 3-4 hours until the optical density at 595 nm (OD600) reached 0.6.
496 Isopropyl-b-D-thiogalactopyranoside (IPTG) was added to the culture to a final concentration
497 of 0.4 mM, and the culture was grown by continuous shaking for 12-16 hours at 16°C. The
498 cells were then harvested by centrifugation, resuspended and sonicated in Strep-Tag washing
499 buffer (100 mM Tris-HCl, 150 mM NaCl, 1 mM EDTA) contaning 1 tablet of cOmplete TM
500 EDTA- free protease inhibitor cocktail (Sigma-Aldrich) per 50 mls of the resuspended cells
501 along with 5 µg/ml DNase I (Sigma-Aldrich). The cell suspension was then disrupted by ultra-
502 sonication on ice using Banddelinuw 3200 (Sonoplus) amplitude (Am) in 35% for 5 sec on and

503 10 sec off for 5-8 minutes. The supernatant containing soluble recombinant protein was
504 harvested following centrifugation at 18,900 x g for 40 mins at 4°C using Sorvall RC Plus with
505 the Fiber-Lite F21 8x50y rotor. Finally, the soluble supernatant was filtered through 0.22 µm
506 pore size filters. After filtration, Strep(II)-tag proteins were purified using affinity column
507 chromatography using a StrepTrap™ column prepacked with StrepTactin Sepharose by
508 following the manufacturer's protocol (GE Healthcare). The VLP recombinant proteins were
509 further purified by size exclusion chromotogrophy (Superose 6, 10/300 GL;GE Healthcare).
510 The level of endotoxin in all the purified VLPs was measured with an ELISA-based endotoxin
511 detection assay (Hyglos) following the manufacturer's protocol.
512 **SDS-PAGE.** The VLP recombinant protein samples were subjected to 10% SDS-PAGE and
513 subsequently characterized by TEM as described previously [20]. Briefly, the VLP
514 recombinant proteins were separated on 10% polyacrylamide gels and stained with instant
515 blue protein stain (Expedeon).
516 ***In vitro* stimulation of BMDCs and BMDMs.** BMDCs were harvested from mice into
517 RPMI 1640© (Sigma-Aldrich) supplemented with 5% heat-inactivated FCS (Hyclone, Logon,
518 UT), 100 µg /mL penicillin and 100 µg/mL streptomycin (Sigma-Aldrich), 2 mM L-Glutamine
519 (Sigma-Aldrich), 50 µM β-mercaptoethanol (Gibco) and 20 ng/ml granulocyte-macrophage
520 colony-stimulating factor (GM-CSF) (eBioscience). BMDMs were harvested from mice into
521 modified Eagle′s Medium (DMEM) – high glucose (Sigma-Aldrich) supplemented with 5%
522 heat-inactivated FCS (Hyclone, Logon, UT), 100 µg/mL penicillin and 100 µg/mL streptomycin
523 (Sigma-Aldrich), Eagle′s minimum essential medium (MEM) non-essential amino acid solution
524 (Sigma-Aldrich), and 0.1 mg/ml macrophage colony-stimulating factor (M-CSF) (eBioscience).
525 BMDMs and BMDCs on day 8 were collected at $1X10^6$/ml and incubated with 10 µg/ml VLP
526 recombinant protein for overnight at 37°C. ES at a final concentration 50 µg/ml and
527 lipopolysaccharide (LPS) at final concentration 0.1 µg/ml were used as positive controls, and
528 untreated cells were used as a negative control. After 24 hours, the supernatants were
529 harvested separately and stored at -20°C until analysed by LEGENDplex for cytokine content
530 according to the manufacturer's instructions.

531 **Fluorescein-conjugated VLP internalization and localization in APCs**. BMDCs and BMMs
532 on day 8 were collected at $1X10^6$/ml and incubated with 10 µg/ml with fluorescein-conjugated
533 VLP separately (HBc-$CBD_{1243-1259}$, HBc-$CBD_{241-257}$, HBc-$CLSP_{143-158}$ and HBc-$CLSP_{398-416}$) for
534 overnight at 37°C in 5% CO_2. Unstimulated BMDCs and BMMs were used as negative
535 controls. Next day, cells were incubated with 50 mM LysoTracker dye obtained from
536 (Invitrogen) for 45 min prior to harvesting to visualise the lysosomal localisation of fluorescein-
537 conjugated VLPs by ImageStreamX cytometry. A Brightfield-1 filter was employed to image
538 dendritic cells and macrophages, a fluorescein isothiocyanate (FITC-488 nm) filter to image
539 fluorescein-conjugated VLPs, and an (APC-592 nm) filter to image lysosomes. The data were
540 analysed using IDEAS software version 6.2.187.0. The degree of co-localization was
541 measured by the Bright Detail Similarity (BDS-R3) on a cell-by-cell basis. A Bright Detail
542 Similarity value of 1.0 indicates a high degree of similarity between two images in the same
543 spatial location (correlated) and a value around 0 has no significant similarity (uncorrelated).
544 **Immunization schedule and challenge infection** Mice were divided randomly into 4 groups:
545 mice were inoculated s.c with overnight ES antigens emulsified with an equal volume of Alum-
546 an aluminum salt adjuvant (88) obtained from Thermo Scientific to achieve a vaccine dose of
547 100 µg ES in 100 µl Alum as a positive control. The negative group was inoculated s.c with
548 200 µl of sterile PBS. Alternatively, mice were vaccinated with 200 µl of 50 µg VLP (HBc-Ag).
549 The vaccinated mouse group was administrated with 200 µl of 50 µg pre-mixed VLPs+T-cell
550 epitopes (HBc-$CBD_{1243-1259}$, HBc-$CBD_{241-257}$, HBc-$CLSP_{143-158}$ and HBc-$CLSP_{398-416}$). All
551 experimental groups were vaccinated in the scruff of the neck at (day -20) and were boosted
552 with the same dose at (day -10) in the same site. At day 10 post vaccination, mice were
553 challenged orally with a high dose of *T. muris* (200 eggs) per mouse. Mice were sacrificed 14
554 days after challenge infection by an overdose of CO_2.
555 **Ag-specific antibody detection in the serum.** Blood samples were collected immediately
556 from mice by cardiac puncture and left at room temperature to clot. Parasite-specific and VLP
557 recombinant protein-specific antibodies (IgM, IgG1 and IgG2c) were determined in sera by
558 enzyme-linked immunosorbent assay (ELISA) as previously described (89). Briefly, 96-well

559 plates were coated with 50 µg/well of the overnight *T. muris* E/S antigen at 5 µg/ml or with 50
560 µg/well of the purified VLP recombinant protein in 0.5 M carbonate-bicarbonate buffer for
561 overnight at 4°C. The plates were washed and then blocked with 3% BSA (Sigma-Aldrich) in
562 PBS Tween-20 (PBS-T20) (0.05% Tween 20, Sigma-Aldrich) for 1 h at 37 °C. After washing,
563 diluted sera were added and incubated for 1 h at 37 °C. Antibody responses were detected
564 using the Biotinylated rat anti-mouse IgM, IgG1 and IgG2a/c (BD Biosciences). After washing,
565 streptavidin peroxidase (Sigma-Aldrich) was added to the plates and incubated for 1 hour at
566 room temperature. The TMB ELISA substrate (3, 3', 5, 5'-tetramethylbenzidine- Thermo) was
567 used to develop color and stopped with 0.003% (H_2SO_4). The optical density at 450 nm with
568 a reference of 570 nm was measured with a Dynex MRX11 plate reader (DYNEX
569 Technologies) at 450 nm with a reference of 570 nm.
570 ***In vitro* stimulation of MLN.** MLNs were harvested from mice at autopsy and dissociated in
571 RPMI-1640 medium (Sigma-Aldrich) supplemented with 10% foetal calf serum (FCS), 1% L-
572 Glutamine, and 1% penicillin/streptomycin (all Invitrogen Ltd., Paisley, UK). $5x10^6$/ml MLN
573 cells were re-stimulated *in vitro* in 96-well plates with 50 µg/ml *T. muris* E/S antigens and with
574 10 µg/ml pre-mixed VLPs+T-cell epitopes proteins (HBc-$CBD_{1243-1259}$, HBc-$CBD_{241-257}$, HBc-
575 $CLSP_{143-158}$, and HBc-$CLSP_{398-416}$) at 37 °C for 48 hours. Cytokine concentration was quantified
576 in the supernatants by cytometric bead array (CBA) according to the manufacturer's
577 instructions from the Mouse/Rat Soluble Protein Flex Set System kit (BD Biosciences
578 Pharmingen, Oxford, UK). CBA data was analysed on a MACSQuant analyser with
579 MACSQuantify™ Software and the CBA analysis software package (BD Biosciences).
580 **Histology.** At autopsy, colonic tissue samples were removed and fixed at room temperature
581 for overnight in 10% neutral buffered formalin, prior to storage in 70% EtOh and processing
582 and embedding in paraffin wax. 5 µm thick serial sections were cut on a Microrn HM325
583 microtome (Microm International, Germany), de-waxed in citroclear and rehydrated prior to
584 periodic acid–Schiff staining. Stained slides of proximal colon sections were scanned using
585 3D Histech Pannoramic 250 flash slide scanner. Photographs of the sections were taken at
586 100X magnification using panoramic viewer version 1.15.4 software. The number of goblet

587 cells was determined as the total number of PAS-positive cells in 60 randomly selected crypts
588 in three fields of view from each section.

589 **Statistics** Statistical analyses were performed using Graph Pad Prism, version 7.00 software.
590 In all tests, P≤0.05 were considered statistically significant and were determined using the
591 Kruskal–Wallis non-parametric ANOVA for comparing multiple groups.

592 Acknowledgments

593 We thank the University of Manchester Histology, Bio-imaging and Flow Cytometry Core
594 Facility for facilitating the image analyses.

595

596 References

597

598 1. Alexander TY, Blackburn BG. Soil-Transmitted Helminths: *Ascaris*, *Trichuris*, and *Hookworm*
599 Infections. Water and Sanitation-Related Diseases and the Environment: In the Age of Climate Change.
600 2019:95.
601 2. WHO WhO. Soil-transmitted helminthiasis: Deworming campaign improves child health,
602 school attendance in Rwanda Geneva: WHO Library. 2015.
603 3. Farrell SH, Coffeng LE, Truscott JE, Werkman M, Toor J, de Vlas SJ, et al. Investigating the
604 Effectiveness of Current and Modified World Health Organization Guidelines for the Control of Soil-
605 Transmitted Helminth Infections. Clinical Infectious Diseases. 2018;66(suppl_4):S253-S9.
606 4. Speich B, Ali SM, Ame SM, Bogoch II, Alles R, Huwyler J, et al. Efficacy and safety of albendazole
607 plus ivermectin, albendazole plus mebendazole, albendazole plus oxantel pamoate, and mebendazole
608 alone against *Trichuris trichiura* and concomitant soil-transmitted helminth infections: a four-arm,
609 randomised controlled trial. The Lancet infectious diseases. 2015;15(3):277-84.
610 5. Jenkins SN, Wakelin D. The source and nature of some functional antigens of *Trichuris muris*.
611 Parasitology. 1977;74(2):153-61.
612 6. Shears RK, Bancroft AJ, Sharpe C, Grencis RK, Thornton DJ. Vaccination Against Whipworm:
613 Identification of Potential Immunogenic Proteins in *Trichuris muris* Excretory/Secretory Material.
614 Scientific reports. 2018;8(1):4508.
615 7. Shears R, Bancroft A, Hughes G, Grencis R, Thornton D. Extracellular vesicles induce protective
616 immunity against *Trichuris muris*. Parasite immunology. 2018:e12536.
617 8. Briggs N, Wei J, Versteeg L, Zhan B, Keegan B, Damania A, et al. *Trichuris muris* whey acidic
618 protein induces type 2 protective immunity against whipworm. PLoS pathogens.
619 2018;14(8):e1007273.
620 9. Geldhof P, De Maere V, Vercruysse J, Claerebout E. Recombinant expression systems: the
621 obstacle to helminth vaccines? Trends in parasitology. 2007;23(11):527-32.
622 10. Hewitson JP, Maizels RM. Vaccination against helminth parasite infections. Expert review of
623 vaccines. 2014;13(4):473-87.
624 11. Del Tordello E, Rappuoli R, Delany I. Reverse Vaccinology: Exploiting Genomes for Vaccine
625 Design. Human Vaccines: Emerging Technologies in Design and Development. 2017:65-86.
626 12. Capecchi B, Serruto D, Adu-Bobie J, Rappuoli R, Pizza M. The genome revolution in vaccine
627 research. Current issues in molecular biology. 2004;6:17-28.
628 13. Moise L, Cousens L, Fueyo J, De Groot AS. Harnessing the power of genomics and
629 immunoinformatics to produce improved vaccines. Expert opinion on drug discovery. 2011;6(1):9-15.

630 14. Arnon R, Ben-Yedidia T. Old and new vaccine approaches. International
631 immunopharmacology. 2003;3(8):1195-204.
632 15. Gregson AL, Oliveira G, Othoro C, Calvo-Calle JM, Thorton GB, Nardin E, et al. Phase I trial of
633 an alhydrogel adjuvanted hepatitis B core virus-like particle containing epitopes of *Plasmodium*
634 *falciparum* circumsporozoite protein. PloS one. 2008;3(2):e1556.
635 16. Roose K, Baets SD, Schepens B, Saelens X. Hepatitis B core–based virus–like particles to
636 present heterologous epitopes. Expert review of vaccines. 2013;12(2):183-98.
637 17. Wynne S, Crowther R, Leslie A. The crystal structure of the human hepatitis B virus capsid.
638 Molecular cell. 1999;3(6):771-80.
639 18. Mosavat A, Soleimanpour S, Farsiani H, Sadeghian H, Ghazvini K, Sankian M, et al. Fused
640 *Mycobacterium tuberculosis* multi-stage immunogens with an Fc-delivery system as a promising
641 approach for the development of a tuberculosis vaccine. Infection, Genetics and Evolution.
642 2016;39:163-72.
643 19. Cabrera-Mora M, Fonseca JA, Singh B, Zhao C, Makarova N, Dmitriev I, et al. A recombinant
644 chimeric Ad5/3 vector expressing a multistage *plasmodium* antigen induces protective immunity in
645 mice using heterologous prime-boost immunization regimens. The Journal of Immunology.
646 2016:1501926.
647 20. Bouchery T, Kyle R, Ronchese F, Le Gros G. The Differentiation of CD4(+) T-Helper Cell Subsets
648 in the Context of Helminth Parasite Infection. Front Immunol. 2014;5:487.
649 21. Dixon H, Little MC, Else KJ. Characterisation of the protective immune response following
650 subcutaneous vaccination of susceptible mice against *Trichuris muris*. International journal for
651 parasitology. 2010;40(6):683-93.
652 22. Dixon H, Johnston C, Else K. Antigen selection for future anti-Trichuris vaccines: a comparison
653 of cytokine and antibody responses to larval and adult antigen in a primary infection. Parasite
654 immunology. 2008;30(9):454-61.
655 23. Else K, Wakelin D, Wassom D, Hauda K. MHC-restricted antibody responses to *Trichuris muris*
656 excretory/secretory (E/S) antigen. Parasite immunology. 1990;12(4-5):509-27.
657 24. Foth BJ, Tsai IJ, Reid AJ, Bancroft AJ, Nichol S, Tracey A, et al. Whipworm genome and dual-
658 species transcriptome analyses provide molecular insights into an intimate host-parasite interaction.
659 Nature genetics. 2014;46(7):693.
660 25. Wang P, Sidney J, Dow C, Mothe B, Sette A, Peters B. A systematic assessment of MHC class II
661 peptide binding predictions and evaluation of a consensus approach. PLoS Comput Biol.
662 2008;4(4):e1000048.
663 26. Wang P, Sidney J, Kim Y, Sette A, Lund O, Nielsen M, et al. Peptide binding predictions for HLA
664 DR, DP and DQ molecules. BMC bioinformatics. 2010;11:568.
665 27. Nielsen M, Justesen S, Lund O, Lundegaard C, Buus S. NetMHCIIpan-2.0-Improved pan-specific
666 HLA-DR predictions using a novel concurrent alignment and weight optimization training procedure.
667 Immunome Res. 2010;6(9):7580-6.
668 28. Nielsen M, Lund O. NN-align. An artificial neural network-based alignment algorithm for MHC
669 class II peptide binding prediction. BMC bioinformatics. 2009;10(1):1.
670 29. Bui HH, Sidney J, Li W, Fusseder N, Sette A. Development of an epitope conservancy analysis
671 tool to facilitate the design of epitope-based diagnostics and vaccines. BMC Bioinformatics.
672 2007;8:361.
673 30. Dimitrov I, Bangov I, Flower DR, Doytchinova I. AllerTOP v. 2—a server for in silico prediction
674 of allergens. Journal of molecular modeling. 2014;20(6):1-6.
675 31. Bancroft AJ, Else KJ, Humphreys NE, Grencis RK. The effect of challenge and trickle *Trichuris*
676 *muris* infections on the polarisation of the immune response. International journal for parasitology.
677 2001;31(14):1627-37.
678 32. King IL, Mohrs K, Meli AP, Downey J, Lanthier P, Tzelepis F, et al. Intestinal helminth infection
679 impacts the systemic distribution and function of the naive lymphocyte pool. Mucosal immunology.
680 2017;10(5):1160.

681 33. Nardin EH, Calvo-Calle JM, Oliveira GA, Nussenzweig RS, Schneider M, Tiercy J-M, et al. A
682 totally synthetic polyoxime malaria vaccine containing *Plasmodium falciparum* B cell and universal T
683 cell epitopes elicits immune responses in volunteers of diverse HLA types. The Journal of Immunology.
684 2001;166(1):481-9.
685 34. Salman AM, Montoya-Díaz E, West H, Lall A, Atcheson E, Lopez-Camacho C, et al. Rational
686 development of a protective *P. vivax* vaccine evaluated with transgenic rodent parasite challenge
687 models. Scientific reports. 2017;7:46482.
688 35. Moura APV, Santos LC, Brito CRN, Valencia E, Junqueira C, Filho AA, et al. Virus-like particle
689 display of the α-Gal carbohydrate for vaccination against *Leishmania infection*. ACS central science.
690 2017;3(9):1026-31.
691 36. Guo J, Zhou A, Sun X, Sha W, Ai K, Pan G, et al. Immunogenicity of a Virus-Like-Particle Vaccine
692 Containing Multiple Antigenic Epitopes of *Toxoplasma gondii* Against Acute and Chronic
693 Toxoplasmosis in Mice. Front Immunol. 2019;10:592.
694 37. Lee S-H, Kim S-S, Lee D-H, Kim A-R, Quan F-S. Evaluation of protective efficacy induced by
695 virus-like particles containing a *Trichinella spiralis* excretory-secretory (ES) protein in mice. Parasites
696 & vectors. 2016;9(1):384.
697 38. Lee D-H, Kim A-R, Lee S-H, Quan F-S. Virus-like particles vaccine containing *Clonorchis sinensis*
698 tegumental protein induces partial protection against *Clonorchis sinensis* infection. Parasites &
699 vectors. 2017;10(1):626.
700 39. Dhanda SK, Usmani SS, Agrawal P, Nagpal G, Gautam A, Raghava GPS. Novel *in silico* tools for
701 designing peptide-based subunit vaccines and immunotherapeutics. Brief Bioinform. 2017;18(3):467-
702 78.
703 40. Yang X, Yu X. An introduction to epitope prediction methods and software. Reviews in medical
704 virology. 2009;19(2):77-96.
705 41. Godkin AJ, Smith KJ, Willis A, Tejada-Simon MV, Zhang J, Elliott T, et al. Naturally processed
706 HLA class II peptides reveal highly conserved immunogenic flanking region sequence preferences that
707 reflect antigen processing rather than peptide-MHC interactions. The Journal of Immunology.
708 2001;166(11):6720-7.
709 42. Lin HH ZG, Tongchusak S, Reinherz EL, Brusic Evaluation of MHC-II peptide binding prediction
710 servers: applications for vaccine research. BMC Bioinformatics. 2008;9:Suppl 12.
711 43. Hegde NR, Gauthami S, Kumar HMS, Bayry J. The use of databases, data mining and
712 immunoinformatics in vaccinology: where are we? Expert Opinion on Drug Discovery. 2018;13(2):117-
713 30.
714 44. Paul S, Arlehamn CSL, Scriba TJ, Dillon MB, Oseroff C, Hinz D, et al. Development and validation
715 of a broad scheme for prediction of HLA class II restricted T cell epitopes. Journal of immunological
716 methods. 2015;422:28-34.
717 45. Schumacher FR, Delamarre L, Jhunjhunwala S, Modrusan Z, Phung QT, Elias JE, et al. Building
718 proteomic tool boxes to monitor MHC class I and class II peptides. Proteomics. 2017;17(1-2).
719 46. Pappalardo F, Flower D, Russo G, Pennisi M, Motta S. Computational modelling approaches to
720 vaccinology. Pharmacol Res. 2015;92:40-5.
721 47. Rammensee H-G, Bachmann J, Emmerich NPN, Bachor OA, Stevanović S. SYFPEITHI: database
722 for MHC ligands and peptide motifs. Immunogenetics. 1999;50(3-4):213-9.
723 48. Reche PA, Glutting J-P, Reinherz EL. Prediction of MHC class I binding peptides using profile
724 motifs. Human immunology. 2002;63(9):701-9.
725 49. Gowthaman U, Agrewala JN. In silico tools for predicting peptides binding to HLA-class II
726 molecules: more confusion than conclusion. Journal of proteome research. 2007;7(01):154-63.
727 50. Borrás-Cuesta F, Golvano J-J, Garcıa-Granero M, Sarobe P, Riezu-Boj J-I, Huarte E, et al. Specific
728 and general HLA-DR binding motifs: comparison of algorithms. Human immunology. 2000;61(3):266-
729 78.
730 51. Lin HH, Ray S, Tongchusak S, Reinherz EL, Brusic V. Evaluation of MHC-II peptide binding
731 prediction servers: applications for vaccine research. BMC bioinformatics. 2008;9((Suppl 12)):10.

732 52. Zhao W, Sher X. Systematically benchmarking peptide-MHC binding predictors: From
733 synthetic to naturally processed epitopes. PLoS Comput Biol. 2018;14(11):e1006457.
734 53. Andreatta M, Trolle T, Yan Z, Greenbaum JA, Peters B, Nielsen M. An automated benchmarking
735 platform for MHC class II binding prediction methods. Bioinformatics. 2018;34(9):1522-8.
736 54. Dobano C, Sanz H, Sorgho H, Dosoo D, Mpina M, Ubillos I, et al. Concentration and avidity of
737 antibodies to different circumsporozoite epitopes correlate with RTS,S/AS01E malaria vaccine
738 efficacy. Nat Commun. 2019;10(1):2174.
739 55. Veronico P, Gray L, Jones J, Bazzicalupo P, Arbucci S, Cortese M, et al. Nematode chitin
740 synthases: gene structure, expression and function in *Caenorhabditis elegans* and the plant parasitic
741 nematode *Meloidogyne artiellia*. Molecular Genetics and Genomics. 2001;266(1):28-34.
742 56. Wei J, Damania A, Gao X, Liu Z, Mejia R, Mitreva M, et al. The hookworm *Ancylostoma*
743 *ceylanicum* intestinal transcriptome provides a platform for selecting drug and vaccine candidates.
744 Parasites & vectors. 2016;9(1):518.
745 57. Foor WE. Ultrastructural aspects of oocyte development and shell formation in *Ascaris*
746 *lumbricoides*. The Journal of parasitology. 1967:1245-61.
747 58. Santos LN, Silva ES, Santos AS, De Sá PH, Ramos RT, Silva A, et al. De novo assembly and
748 characterization of the *Trichuris trichiura* adult worm transcriptome using Ion Torrent sequencing.
749 Acta tropica. 2016;159:132-41.
750 59. Johnston WL, Krizus A, Dennis JW. The eggshell is required for meiotic fidelity, polar-body
751 extrusion and polarization of the *C. elegans* embryo. BMC biology. 2006;4(1):35.
752 60. Johnston WL, Krizus A, Dennis JW. Eggshell chitin and chitin-interacting proteins prevent
753 polyspermy in *C. elegans*. Current Biology. 2010;20(21):1932-7.
754 61. Cuesta-Astroz Y, de Oliveira FS, Nahum LA, Oliveira G. Helminth secretomes reflect different
755 lifestyles and parasitized hosts. International journal for parasitology. 2017;47(9):529-44.
756 62. Balasubramanian N, Toubarro D, Simoes N. Biochemical study and in vitro insect immune
757 suppression by a trypsin-like secreted protease from the nematode Steinernema carpocapsae.
758 Parasite immunology. 2010;32(3):165-75.
759 63. Santos LN, Gallo MB, Silva ES, Figueiredo CAV, Cooper PJ, Barreto ML, et al. A proteomic
760 approach to identify proteins from *Trichuris trichiura* extract with immunomodulatory effects. Parasite
761 immunology. 2013;35(5-6):188-93.
762 64. Yang Y, jun Wen Y, Cai YN, Vallée I, Boireau P, Liu MY, et al. Serine proteases of parasitic
763 helminths. The Korean journal of parasitology. 2015;53(1):1.
764 65. Toubarro D, Lucena-Robles M, Nascimento G, Santos R, Montiel R, Veríssimo P, et al. Serine
765 protease-mediated host invasion by the parasitic nematode Steinernema carpocapsae. Journal of
766 biological chemistry. 2010:jbc. M110. 129346.
767 66. Dalton JP, Brindley PJ, Knox DP, Brady CP, Hotez PJ, Donnelly S, et al. Helminth vaccines: from
768 mining genomic information for vaccine targets to systems used for protein expression. International
769 journal for parasitology. 2003;33(5-6):621-40.
770 67. Wang B, Wang ZQ, Jin J, Ren HJ, Liu LN, Cui J. Cloning, expression and characterization of a
771 *Trichinella spiralis* serine protease gene encoding a 35.5 kDa protein. Experimental parasitology.
772 2013;134(2):148-54.
773 68. Feng S, Wu X, Wang X, Bai X, Shi H, Tang B, et al. Vaccination of mice with an antigenic serine
774 protease-like protein elicits a protective immune response against *Trichinella spiralis* infection. The
775 Journal of parasitology. 2013;99(3):426-32.
776 69. Xu J, Bai X, Wang LB, Shi HN, Van Der Giessen JW, Boireau P, et al. Immune responses in mice
777 vaccinated with a DNA vaccine expressing serine protease-like protein from the new-born larval stage
778 of *Trichinella spiralis*. Parasitology. 2017;144(6):712-9.
779 70. Serradell MC, Rupil LL, Martino RA, Prucca CG, Carranza PG, Saura A, et al. Efficient oral
780 vaccination by bioengineering virus-like particles with protozoan surface proteins. Nature
781 Communications. 2019;10(1):361.

71. Wahl-Jensen V, Kurz SK, Hazelton PR, Schnittler H-J, Ströher U, Burton DR, et al. Role of Ebola virus secreted glycoproteins and virus-like particles in activation of human macrophages. Journal of virology. 2005;79(4):2413-9.
72. Lahoud MH, FatmaKitsoulis, SusieSan Wan, SooVremec, DavidLee, Chin-NienPhipson, BelindaShi, WeiSmyth, Gordon K, Lew AM. Targeting antigen to mouse dendritic cells via Clec9A induces potent CD4 T cell responses biased toward a follicular helper phenotype. The Journal of Immunology. 2011(2):842-50.
73. Birkett A, Thornton B, Milich D, Oliveira G, Siddique A, Nussenzweig R, et al. Hepatitis B virus core antigen particles containing minimal T and B cell epitopes of *Plasmodium falciparum* CS protein elicit high levels of malaria specific immune responses in mice and non-human primates. Am J Trop Med Hyg. 2001;65:258.
74. Birkett A, Lyons K, Schmidt A, Boyd D, Oliveira G, Siddique A, et al. A modified hepatitis B virus core particle containing multiple epitopes of the *Plasmodium falciparum* circumsporozoite protein provides a highly immunogenic malaria vaccine in preclinical analyses in rodent and primate hosts. Infection and immunity. 2002;70(12):6860-70.
75. Milich DR, Hughes J, Jones J, Sällberg M, Phillips TR. Conversion of poorly immunogenic malaria repeat sequences into a highly immunogenic vaccine candidate. Vaccine. 2001;20(5-6):771-88.
76. Nardin EH, Oliveira GA, Calvo-Calle JM, Wetzel K, Maier C, Birkett AJ, et al. Phase I testing of a malaria vaccine composed of hepatitis B virus core particles expressing *Plasmodium falciparum* circumsporozoite epitopes. Infection and immunity. 2004;72(11):6519-27.
77. Oliveira GA, Wetzel K, Calvo-Calle JM, Nussenzweig R, Schmidt A, Birkett A, et al. Safety and enhanced immunogenicity of a hepatitis B core particle *Plasmodium falciparum* malaria vaccine formulated in adjuvant Montanide ISA 720 in a phase I trial. Infection and immunity. 2005;73(6):3587-97.
78. Gu Y, Huang J, Wang X, Wang L, Yang J, Zhan B, et al. Identification and characterization of CD4+ T cell epitopes present in Trichinella spirals paramyosin. Veterinary parasitology. 2016;231:59-62.
79. Datta R, Hedeler C, Paton N, Brass A, Else K. Identification of novel genes in intestinal tissue that are regulated after infection with an intestinal nematode parasite. Infection and immunity. 2005;73(7):4025-33.
80. Hasnain SZ, Wang H, Ghia JE, Haq N, Deng Y, Velcich A, et al. Mucin gene deficiency in mice impairs host resistance to an enteric parasitic infection. Gastroenterology. 2010;138(5):1763-71. e5.
81. Hasnain SZ, McGuckin MA, Grencis RK, Thornton DJJPNTD. Serine protease(s) secreted by the nematode Trichuris muris degrade the mucus barrier. 2012;6.
82. Moher D, Liberati A, Tetzlaff J, Altman DG, Group P. Preferred reporting items for systematic reviews and meta-analyses: the PRISMA statement. International journal of surgery. 2010;8(5):336-41.
83. Yasser E-M, Dobbs D, Honavar V. On evaluating MHC-II binding peptide prediction methods. PloS one. 2008;3(9):e3268.
84. Murugan N, Dai Y. Prediction of MHC class II binding peptides based on an iterative learning model. Immunome research. 2005;1(1):6.
85. Nielsen M, Lundegaard C, Worning P, Hvid CS, Lamberth K, Buus S, et al. Improved prediction of MHC class I and class II epitopes using a novel Gibbs sampling approach. Bioinformatics. 2004;20(9):1388-97.
86. Altman DG, Bland JM. Diagnostic tests. 1: Sensitivity and specificity. BMJ: British Medical Journal. 1994;308(6943):1552.
87. Wakelin DJP. Acquired immunity to *Trichuris muris* in the albino laboratory mouse. 1967;57(3):515-24.
88. HogenEsch H. Mechanism of immunopotentiation and safety of aluminum adjuvants. Frontiers in immunology. 2013;3:406.

89. Else K, Entwistle G, Grencis R. Correlations between worm burden and markers of Th1 and Th2 cell subset induction in an inbred strain of mouse infected with *Trichuris muris*. Parasite immunology. 1993;15(10):595-600.

Supporting Information Legends

S1 Fig. The HBc-antigen fusion recombinant protein purification and assembly. Left: Chromatogram of the VLP recombinant proteins HBc-Ag (A), HBc-CBD$_{1243-1259}$ (B), HBc-CBD$_{241-257}$ (C), HBc-CLSP$_{143-158}$, (D), and HBc-CLSP$_{398-416}$ (E) purified using SEC. Separation was carried out on a Superose 6, 10/300 GL (GE Healthcare), at a flow rate of 0.2 ml/min with 100 mM Tris-HCl, 150 mM NaCl, 1 mM EDTAatpH 8. VLP recombinant proteins were eluted in 0.5 ml fraction and a sample of SEC the elution peak was visualised by SDS-PAGE. Vertical red lines indicate the elution volume of mass standards, from left to right: 2MDa, 670kDa. Right: Purification visualised by SDS-PAGE (10% gel) analysis stained with Coomassie blue. M: protein marker (Precision Plus protein standard, unstained, Bio-Rad); Lane 1: VLP recombinant protein after Strep-Tag affinity purification using the StrepTrap HP, and Lane 2: VLP recombinant protein after SEC purification. The arrow represents VLP recombinant protein monomer with an expected molecular mass of ~22 kDa.

S2 Fig. Cytokine productions by mesenteric lymph node cells and quantification of goblet cell numbers in mice vaccinated with VLPs+T-cell epitopes and control mice. (A) MLNs from mice vaccinated with 50 µg of pre-mixed of VLPs+T-cell epitopes epitopes (HBc-CBD$_{1243-1259}$, HBc-CBD$_{241-257}$, HBc-CLSP$_{143-158}$ and HBc-CLSP$_{398-416}$), 50 µg of VLP (HBc-Ag), 50 µg ES/Alum, or PBS on day -20 and boosted on day -10 were stimulated at 5x10^6/ml with 50 µg/ml *T. muris* ES. After 48 hours of stimulation, cell culture supernatants were harvested and assayed by cytometric bead array for IL-4 (A), IL-6 (B), IL-10 (C), IL-17 (D), and TNF (E) production. Statistical analyses were carried out using the Kruskal-Wallis test (multiple comparisons). Significant differences between groups are represented by (*P≤0.05) with a line. Results are shown as mean ± SEM. n= 11 mice per group. The results presented are from two separated experiment pooled together.

S1 Table. List of Keywords used to screen for MHC I and II *in silico* prediction tools.

S2 Table. List of MHC class I and II and HLA binders peptides *in silico* prediction tools.

S3 Table. MHC-II T-cell epitopes dataset used to evaluate the MHC-II *in silico* prediction tools.

S4 Table. List of MHC-II T-cell epitope sequences and primers used to amplify the target.

Figure Legends

Fig 1. (A) PRISMA flow diagram of the systematic review screening process for restricted MHC-II T-cell bioinformatics prediction tools. A list of search terms was used in Google website and other website sources to screen for MHC class I and II *in silico* prediction tools. Aspects relating to the number of citations (>200), number of publications, online availability, last update and community were used as inclusion/exclusion criteria to select the top MHC-II *in silico* prediction tools. n= number of key words, websites sources and *in silico* prediction tools. (B) The flow diagram of reverse vaccinology approach to identify potential vaccine candidates (MHC-II T-cell epitopes) from the *T. muris* genome. The number on the arrow represents the number of proteins or epitopes selected for the next step. (C) List of 4 *Trichuris* MHC-II T-cell epitopes which have potential as vaccine candidates.

Fig 2. (A) Inflammatory cytokines production by mouse bone marrow-derived DCs (BMDCs) and mouse bone marrow-derived macrophages (BMDMs) (B) in response to VLPs. BMDCs and BMDMs at 1X10^6/ml were stimulated *in vitro* with 10 µg/ml VLPs (HBc-Ag, HBc-H$_{112-128}$, HBc-CBD$_{1243-1259,}$ HBc-CBD$_{241-257}$, HBc-CLSP$_{143-158}$ and HBc-CLSP$_{398-416}$) and with 50 µg/ml ES and 0.1 µg/ml LPS as positive controls. Unstimulated BMDCs and BMDMs served as negative controls. Supernatants were harvested after 24 hours for IL-6 and TNF α

886 cytokine analyses measured by CBA. The bars represent mean ± SEM. Statistical analyses
887 were carried out using the Kruskal-Wallis test (multiple comparisons). Significant differences
888 between groups are represented by (*P≤0.05) with a line. Chart bars represent BMDCs and
889 BMDMs grown from three individual mice from one representative experiment of two separate
890 experiments. (C) Representative images of fluorescein-conjugated VLPs internalisation in the
891 BMDCs and BMDMs (G). BMDCs and BMDMs at $1X10^6$/ml were incubated with 10 µg/ml
892 fluorescein-conjugated VLP (HBc-Ag and HBc-$CLSP_{398-416}$) for 24 hours. As a negative
893 control, unstimulated BMDCs and BMDMs were examined. Cell internalisation was
894 determined by Amnis ImageStreamX cytometer compared to unstimulated BMDCs and
895 BMDMs. Images shown, from left to right, show individual Brightfield images (BF) in the white
896 channel, fluorescent-labelled stimulus (FITC) in the green channel and the combination of both
897 BF/FITC merged channels. The internalisation mean absolute deviation (MAD) is included
898 above its images. The positive MAD value represents internalisation, and negative values
899 represent poor internalisation. (D) Representative images of fluorescein-conjugated VLPs co-
900 localization in the BMDCs and BMDMs (H). BMDCs and BMDMs at $1X10^6$/ml were stained
901 with Lysotracker to visualise the cellular lysosome compartment and subsequently stimulated
902 with 10 µg/ml fluorescein-conjugated VLP (HBc-Ag, and HBc-$CLSP_{398-416}$) for 24 hours. As a
903 negative control, unstimulated BMDCs and BMDMs were examined. Intracellular co-
904 localization was determined by Amnis ImageStreamX cytometer. Images shown, from left to
905 right, show individual Brightfield images (BF) in the white channel, fluorescent-labelled
906 stimulus (FITC) in the green channel, stained lysosome (Lysotracker) in the red channel and
907 the combination of both FITC/ Lysotracker merged channels. The Similarity bright detail score
908 (SBDS) from the IDEAS quantitative co-localization analysis is included above its image.
909 SBDS values around 1 represent co-localization, and 0 values represent poor co-localization.
910 Scale bars represent 10 µm.
911
912
913 **Fig 3. Experimental schedule, worm burden, parasite-specific and VLP-specific**
914 **antibodies levels of mice vaccinated and challenged with a *T. muris* infection.** 6-week
915 old male C57BL/6 mice were vaccinated subcutaneously with 50 µg of pre-mixed of VLPs+T-
916 cell epitopes (HBc-$CBD_{1243-1259}$, HBc-$CBD_{241-257}$, HBc-$CLSP_{143-158}$, and HBc-$CLSP_{398-416}$), 50 µg
917 of VLP (HBc-Ag), or PBS on day -20 and boosted on day -10. Mice were infected by oral
918 gavage with approximately 150 infective *T. muris* eggs on day 0 and sacrificed at d14 post-
919 infection. (B) Comparison of worm burden at day 14 post-infection. (C) Worm burden in mice
920 vaccinated with 50 µg of ES. n= 11 mice per group. The results presented are from two
921 separated experiments pooled together. Day 14 p.i. sera were titrated against *T. muris* ES
922 antigens to assess parasite-specific IgM (D) IgG1 (E), and IgG2c (F) levels in VLPs+T-cell
923 epitopes, VLP (HBc-Ag), PBS and in ES vaccinated mice by ELISA (reading at 405 nm). Day
924 14 p.i. sera were titrated against premixed VLPs+ T- cell epitopes antigens to assess VLPs+
925 T- cell epitopes-specific IgM (G) IgG1 (H), and IgG2c (I) levels in VLPs+T-cell epitopes, VLP
926 (HBc-Ag), PBS and in ES vaccinated mice. Statistical analyses were carried out using Kruskal-
927 Wallis test (multiple comparisons). Significant differences between groups are represented by
928 (*P≤0.05, **P≤0.01, ***P≤0.001, ****P≤0.0001) with a line. Results are shown as mean ± SEM.
929 n= 6 mice per group. This experiment was repeated two times, and the ELISA results shown
930 here are representative of the two experiments.
931
932 **Fig 4. Cytokine productions by mesenteric lymph node cells and quantification of**
933 **goblet cell numbers in mice vaccinated with VLPs+T-cell epitopes and control mice.** (A)
934 MLNs from mice vaccinated with 50 µg of pre-mixed of VLPs+T-cell epitopes epitopes (HBc-
935 $CBD_{1243-1259}$, HBc-$CBD_{241-257}$, HBc-$CLSP_{143-158}$ and HBc-$CLSP_{398-416}$), 50 µg of VLP (HBc-Ag),
936 50 µg ES/Alum, or PBS on day -20 and boosted on day -10 were stimulated at $5x10^6$/ml with
937 50 µg/ml *T. muris* ES. After 48 hours of stimulation, cell culture supernatants were harvested
938 and assayed by cytometric bead array for IL-5 (A), IL-9 (B), IL-13 (C), IFN-□ (D) production.
939 (E) Representative photographs of gut sections stained with Periodic acid–Schiff staining
940 (PAS). The slides were scanned, and the goblet cells were quantified using Panoramic Viewer

941 software. All photographs were taken with 20X magnification. (F) Goblet cells were quantified
942 by counting the number of alcian blue-stained cells per crypt unit in three fields of view from
943 each section and are shown as mean cell numbers per 20 crypt units (cu) ±SEM. Statistical
944 analyses were carried out using the Kruskal-Wallis test (multiple comparisons). Significant
945 differences between groups are represented by (*P≤0.05, ****P≤0.0001) with a line. Results
946 are shown as mean ± SEM. n= 11 mice per group. The results presented are from two
947 separated experiment pooled together.
948

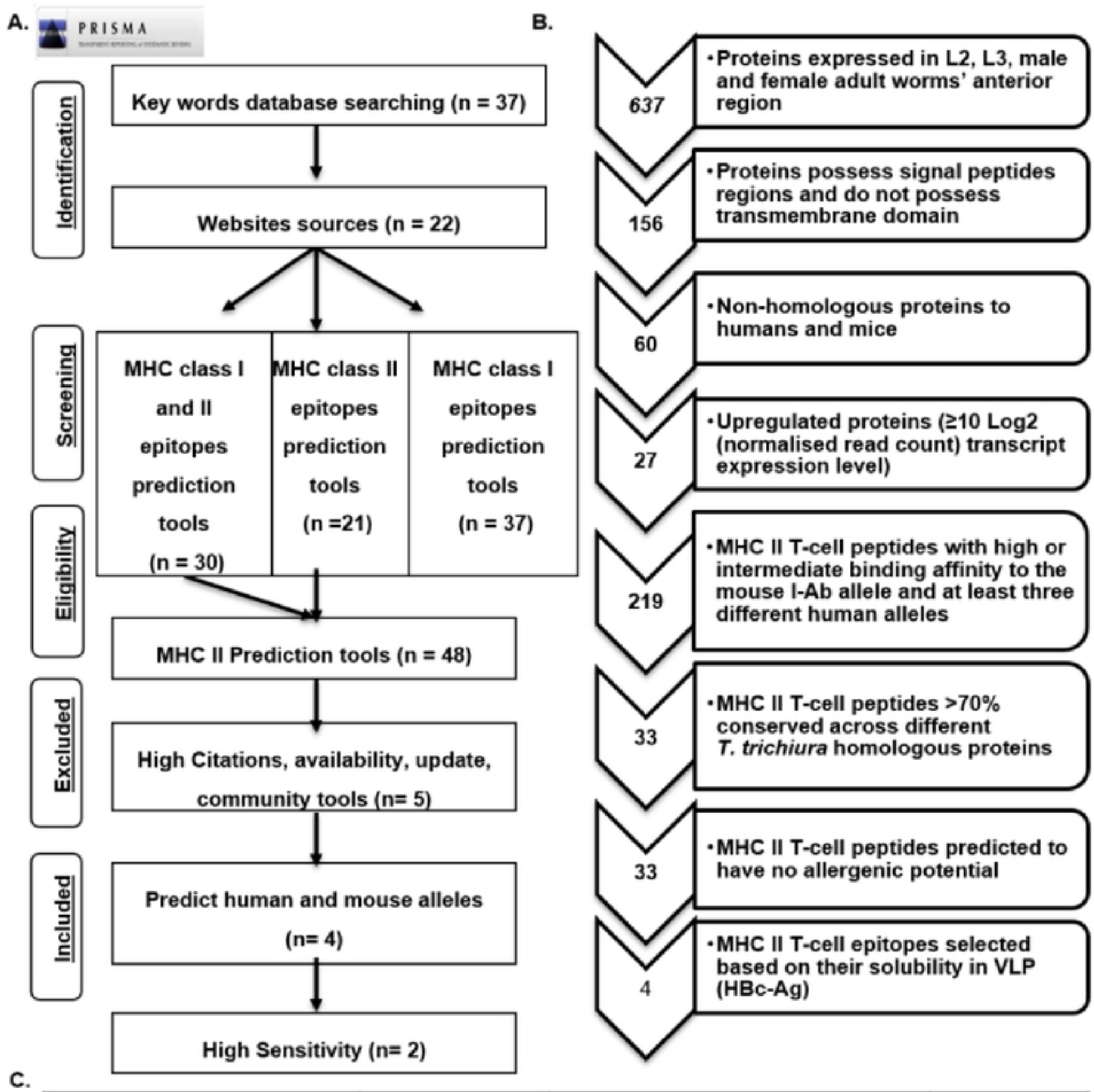

T. muris protein (UniProt ID)	Epitope name	Peptide sequence	Amino acid position
Chymotrypsin-like serine protease (A0A0N5DUC1)	CLSP143-158	AILQLAKPVPFSNTVR	143-158
Chymotrypsin-like serine protease (A0A0N5DUC1)	CLSP398-416	CTGSLYASARANFTRTVLTS	398-416
Chitin-binding domain containing protein (A0A0N5E6C6)	CBD1243-1259	PAGVVYQCTMPRYTLCV	1243-1259
Chitin-binding domain containing protein (A0A0N5DK22)	CBD241-257	GRTTPVTSAPTTVTTER	241-257

Figure 1

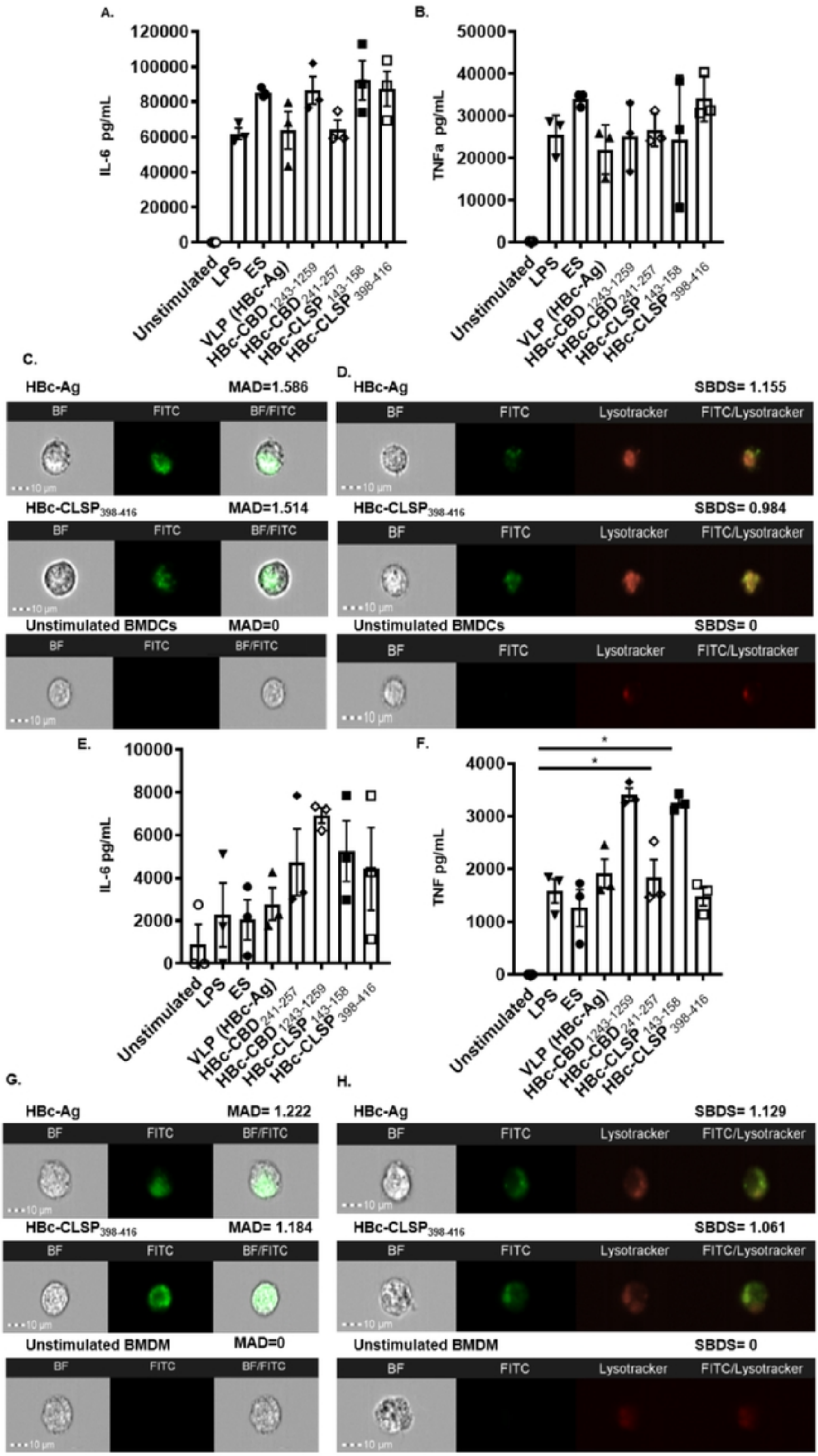
A.
IL-6 pg/mL
120000
100000
80000
60000
40000
20000
0
Unstimulated
LPS
ES
VLP (HBc-Ag)
HBc-CBD 1243-1259
HBc-CBD 241-257
HBc-CLSP 143-158
HBc-CLSP 398-416
B.
TNFa pg/mL
50000
40000
30000
20000
10000
0
C.
HBc-Ag
MAD=1.586
HBc-CLSP398-416
MAD=1.514
Unstimulated BMDCs
MAD=0
BF
FITC
BF/FITC
D.
HBc-Ag
SBDS= 1.155
HBc-CLSP398-416
SBDS= 0.984
Unstimulated BMDCs
SBDS= 0
Lysotracker
FITC/Lysotracker
10 µm
E.
IL-6 pg/mL
10000
8000
6000
4000
2000
0
F.
TNF pg/mL
4000
3000
2000
1000
0
*
*
G.
HBc-Ag
MAD= 1.222
HBc-CLSP398-416
MAD= 1.184
Unstimulated BMDM
MAD=0
H.
HBc-Ag
SBDS= 1.129
HBc-CLSP398-416
SBDS= 1.061
Unstimulated BMDM
SBDS= 0

Figure 2

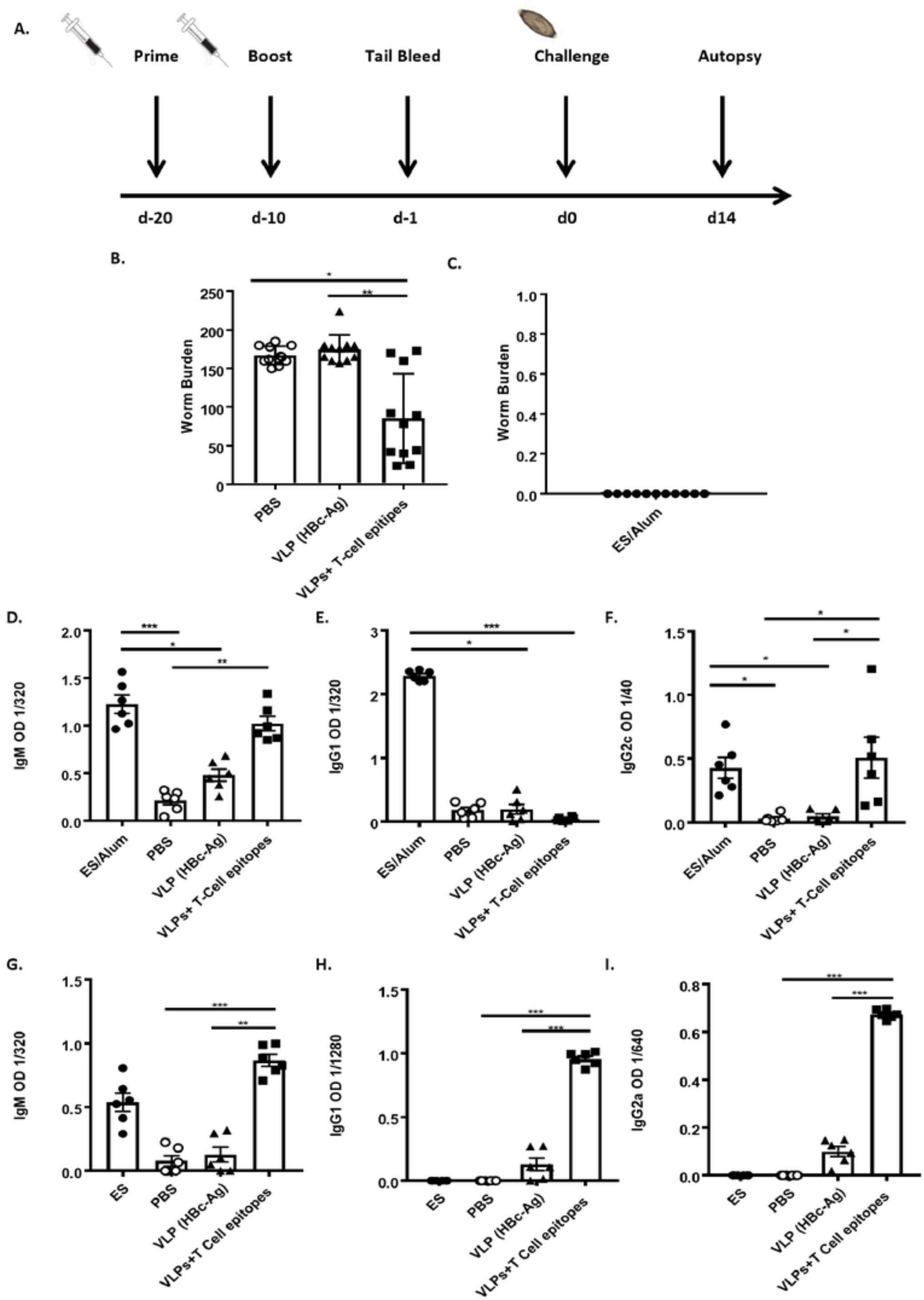
A.
Prime
Boost
Tail Bleed
Challenge
Autopsy
d-20
d-10
d-1
d0
d14
B.
Worm Burden
PBS
VLP (HBc-Ag)
VLPs+ T-cell epitipes
C.
Worm Burden
ES/Alum
D.
IgM OD 1/320
ES/Alum
PBS
VLP (HBc-Ag)
VLPs+ T-Cell epitopes
E.
IgG1 OD 1/320
F.
IgG2c OD 1/40
G.
IgM OD 1/320
ES
PBS
VLP (HBc-Ag)
VLPs+T Cell epitopes
H.
IgG1 OD 1/1280
I.
IgG2a OD 1/640

Figure 3

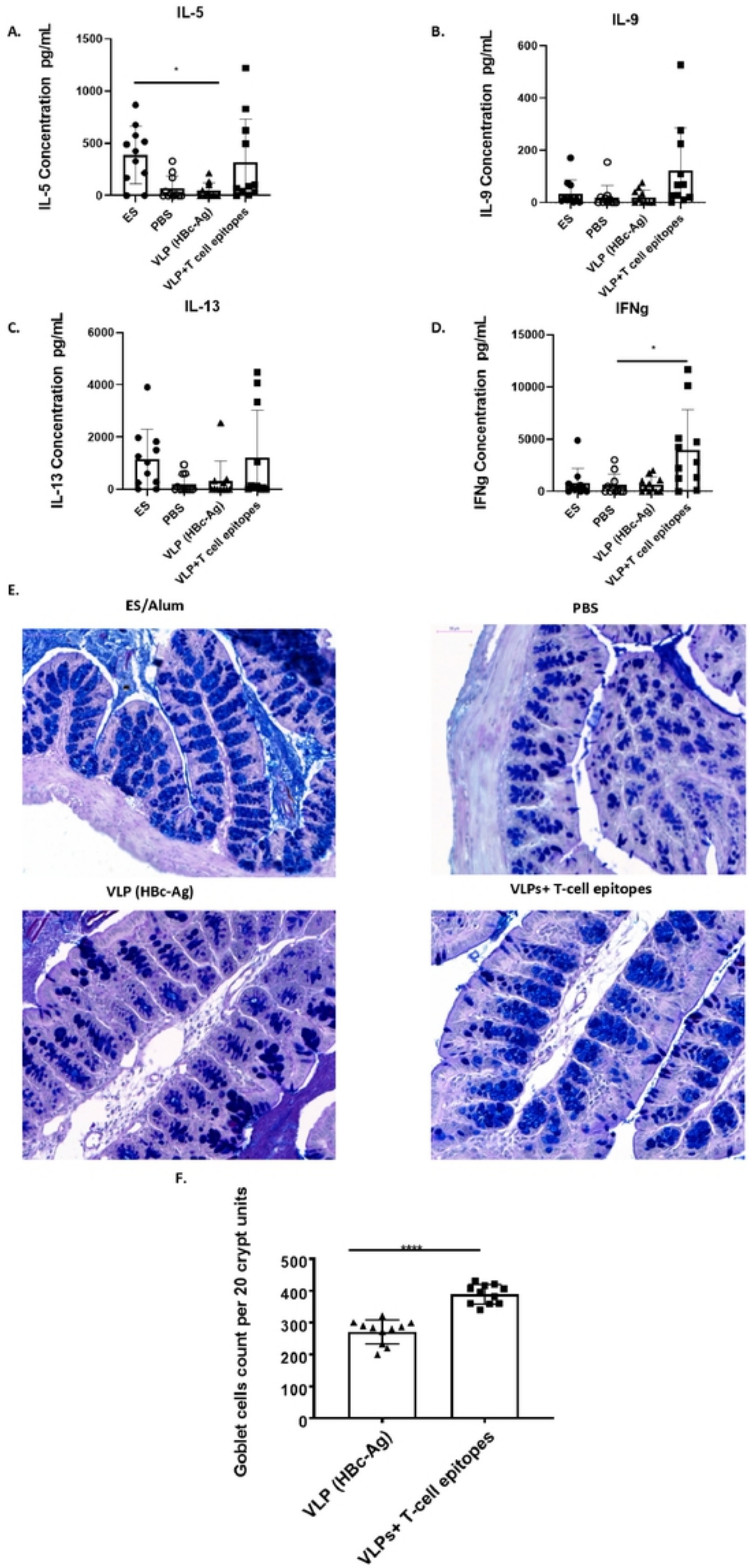
A.
IL-5
IL-5 Concentration pg/mL
1500
1000
500
0
ES
PBS
VLP (HBc-Ag)
VLP+T cell epitopes
B.
IL-9
IL-9 Concentration pg/mL
600
400
200
0
ES
PBS
VLP (HBc-Ag)
VLP+T cell epitopes
C.
IL-13
IL-13 Concentration pg/mL
6000
4000
2000
0
ES
PBS
VLP (HBc-Ag)
VLP+T cell epitopes
D.
IFNg
IFNg Concentration pg/mL
15000
10000
5000
0
ES
PBS
VLP (HBc-Ag)
VLP+T cell epitopes
E.
ES/Alum
PBS
VLP (HBc-Ag)
VLPs+ T-cell epitopes
F.
Goblet cells count per 20 crypt units
****
500
400
300
200
100
0
VLP (HBc-Ag)
VLPs+ T-cell epitopes

Figure 4